Delft University of Technology

Revealing the Transient Concentration of CO_2 in a Mixed-Matrix Membrane by IR Microimaging and Molecular Modeling

Hwang, Seungtaik; Semino, Rocio; Seoane, Beatriz; Zahan, Marufa; Chmelik, Christian; Valiullin, Rustem; Bertmer, Marko; Haase, Jürgen; Kapteijn, Freek; Gascon, Jorge

Important note
To cite this publication, please use the final published version (if applicable).
Please check the document version above.

Revealing the Transient Concentration of CO_2 in a Mixed-Matrix Membrane by IR Microimaging and Molecular Modeling

Seungtaik Hwang, Rocio Semino, Beatriz Seoane, Marufa Zahan, Christian Chmelik, Rustem Valiullin, Marko Bertmer, Jürgen Haase, Freek Kapteijn, Jorge Gascon, Guillaume Maurin,* and Jörg Kärger*

Abstract: *Through IR microimaging the spatially and temporally resolved development of the CO_2 concentration in a ZIF-8@6FDA-DAM mixed matrix membrane (MMM) was visualized during transient adsorption. By recording the evolution of the CO_2 concentration, it is observed that the CO_2 molecules propagate from the ZIF-8 filler, which acts as a transport "highway", towards the surrounding polymer. A high-CO_2-concentration layer is formed at the MOF/polymer interface, which becomes more pronounced at higher CO_2 gas pressures. A microscopic explanation of the origins of this phenomenon is suggested by means of molecular modeling. By applying a computational methodology combining quantum and force-field based calculations, the formation of microvoids at the MOF/polymer interface is predicted. Grand canonical Monte Carlo simulations further demonstrate that CO_2 tends to preferentially reside in these microvoids, which is expected to facilitate CO_2 accumulation at the interface.*

Recent trends in mixed-matrix membranes (MMMs) have led to remarkable progress on MMM preparation techniques and a proliferation of new metal–organic framework (MOF)-based MMMs with enhanced separation performance overcoming the limitation of pure polymeric membranes, namely the inevitable trade-off between guest-molecule permeability and selectivity.[1] Most of the applications of such composites are closely related/subject to the rate of molecular mass transfer between the internal pore system and their surrounding gas phase. Despite the significant development of new MMM generations, relatively few fundamental studies dealing with the limiting steps of intrinsic mass transfer of guest molecules in MMMs and their quantitation have been published. As a consequence, causal factors associated with CO_2 uptake in the two different phases, that is, fillers and polymer, within MMMs still remain speculative. A thorough investigation of the interfacial structures of MMMs and the individual and/or integrated effects of the two components on the overall uptake of guest molecules in the composites, which became possible recently along with molecular modeling[2] and microimaging by infrared microscopy (IRM),[3] is therefore considered as a prerequisite for a rational design of industrial-scale MMMs with optimum performance. To achieve optimum transport properties of MMMs, in particular, exploitation of the interfacial contact zone between fillers and polymer is very important.[4] Depending on the interaction of fillers with surrounding polymer, 1) a nanometer-sized void phase, appearing as a gap, can be formed between the two components[4,5] or 2) structural modification of the polymer can occur in close proximity to the fillers, which is known as the polymer "hardening effect".[6] Among the numerous models in literature,[7] which are mostly derived or developed from Maxwell's equation[8] to predict the permeability of MMMs, a rigorous modeling approach recently proposed by Petropoulos et al.[6] specifically takes into account the third phase, that is, the "interphase" between fillers and polymer.

Herein we focus on the application of the IR microimaging technique to record the CO_2 concentration and its variation in space and time within a MMM consisting of a 150 µm-thick 6FDA-DAM polymer film and large ZIF-8 crystals[9] (2.5 wt %) over 70 µm. These characteristics differ from those of commercially used membranes (a thickness of 0.1 to 1 µm and a MOF-to-polymer ratio from 1:10 to 1:3). It is a consequence of the limitations in sensitivity and spatial resolution of IR microimaging. The use of giant crystals, moreover, lifts the limitations in the temporal resolution of IR microimaging since the time constant of local equilibration increases with the square of the crystal size.[10] This enables a microscopic view of guest distributions under non-equilibrium conditions to be attained, which may serve as a first-order approach of the non-equilibrium conditions finally

[*] S. Hwang, M. Zahan, Dr. C. Chmelik, Dr. R. Valiullin, Dr. M. Bertmer,
Prof. J. Haase, Prof. J. Kärger
Faculty of Physics and Earth Sciences
University of Leipzig
Linnéstrasse 5, 04103 Leipzig (Germany)
E-mail: kaerger@physik.uni-leipzig.de

Dr. R. Semino, Prof. G. Maurin
Institut Charles Gerhardt Montpellier
Université de Montpellier
Place Eugène Bataillon, 34095 Montpellier Cedex 5 (France)
E-mail: Guillaume.Maurin@univ-montp2.fr

Dr. R. Semino
Institute of Materials, École Polytechnique Fédérale de Lausanne
Route Cantonale, 1015 Lausanne (Switzerland)

Dr. B. Seoane
Debye Institute for Nanomaterials Science, Utrecht University
Universiteitsweg 99, 3584 CG Utrecht (The Netherlands)

Dr. B. Seoane, Prof. F. Kapteijn, Prof. J. Gascon
Catalysis Engineering, ChemE Department, Delft University of
Technology
Van der Maasweg 9, 2629 HZ Delft (The Netherlands)

Prof. J. Gascon
Advanced Catalytic Materials, KAUST Catalysis Center, King Abdullah
University of Science and Technology
Thuwal 23955-6900 (Saudi Arabia)

Supporting information and the ORCID identification number(s) for the author(s) of this article can be found under:
https://doi.org/10.1002/anie.201713160.

5156 **Wiley Online Library**

© 2018 Wiley-VCH Verlag GmbH & Co. KGaA, Weinheim

Angew. Chem. Int. Ed. **2018**, *57*, 5156 –5160

attained during the stationary use of real membranes. Detailed information of the sample preparation procedures is given in Supporting Information. The same type of the MMM, that is, a combination of 6FDA-DAM polymer and 200 nm commercial ZIF-8 crystals (Basolite Z1200, BASF), was already studied, demonstrating its great potential for the C_3H_6/C_3H_8 separation process.[11]

The IR microimaging technique enables us to monitor the propagation of CO_2 molecules during transient adsorption and their location, for example, in filler, polymer, or interfacial region, at equilibrium. In fact, the information given by IR microimaging is the CO_2 concentration integral along the IR light pathway, that is, the z-direction, throughout the (x–y) observation plane with a spatial resolution of approximately 3 μm.[9] This is not exactly the "local" CO_2 concentration, but given the fact that such MMMs exhibit uniform thickness and good compositional homogeneity,[12] that is, no significant variation in the local CO_2 concentration along the z-direction, the concentration integral may differ only slightly from the local concentration by a factor of proportionality and could be indeed considered as a "localized" CO_2 concentration over the (x-y) observation plane.

Figure 1a shows the ZIF-8@6FDA-DAM MMM located in the measurement window of the IR microscope with a size of around 145 μm × 340 μm in Viewing Mode.[3a] The dimensions of the crystal embedded into the polymer are about 110 μm and 140 μm in the x- and the y-directions, respectively. Considering the typical shape of ZIF-8 which is rhombic dodecahedral, the thickness of the crystal is assumed to be of the same order of magnitude. In addition to the thickness, the absence of roughness or a bump on the MMM′s surface ensured that the crystal was located within the polymer without any exposure to the atmosphere. As shown in Figure 1b which is a colored contour map of ZIF-8 content, there is only a single ZIF-8 crystal within the measurement window. The contour map was produced by integrating IR light absorbance spectra over a characteristic IR band[13] of ZIF-8, which was near 3140 cm^{-1}. The surrounding polymer colored in blue in the map (Figure 1b) indicates that there are no small, powder-like ZIF-8 crystals present in the current
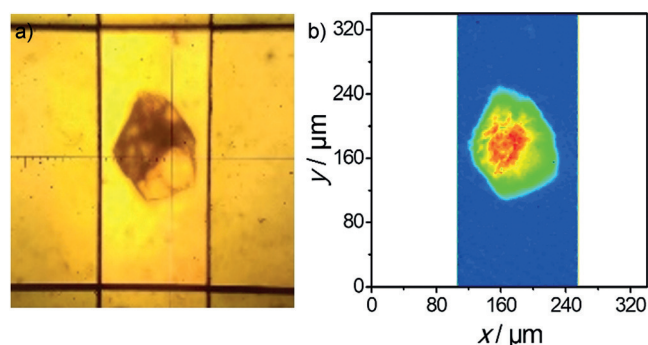
measurement window. This observation was also confirmed by comparing the IR light absorbance spectra of different areas around the crystal (see Supporting Information and Figure S3). The red color at the center of the crystal (Figure 1b) illustrates that its center is thicker than its boundary.

In addition to Figures 1a,b, a focused ion beam–scanning electron microscopy (FIB-SEM) micrograph of the same type of the MMM (Figure S2) also shows no apparent empty gap between the fillers and the polymer. Although it is often used to assess the quality of the polymer–filler interface in MMMs, it does not provide us with a complete picture of the interfacial inhomogeneity and defects at the nanometer scale. To evaluate the nature of the polymer–filler interactions and their microscopic compatibility, molecular simulations and solid-state nuclear magnetic resonance spectroscopy will be employed later in the present study.

Figure 2 provides a series of time-resolved images of CO_2 concentration as captured by IR microimaging during the uptake of CO_2 in the ZIF-8@6FDA-DAM MMM (see Supporting Information). The filler ZIF-8 is clearly seen to reach equilibrium within 100 s (Figure 2b) since the commencement of the uptake, and its CO_2 concentration does not vary significantly until the end of the experiment. This behavior is expected, considering the intracrystalline diffusivity of ZIF-8 of an order of 10^{-10} $m^2 s^{-1}$[14] and its size. At equilibrium (Figure 2h), the polymer exhibits a higher CO_2 loading than the filler as expected from the CO_2 adsorption isotherms of the two components (Figure S4). It is also noticeable in Figure 2a–d that the CO_2 molecules propagate from the filler to the surrounding 6FDA-DAM polymer. The filler thus appears to act as a "highway" for CO_2 mass transport, thereby accelerating the overall uptake or the permeance of CO_2 in the MMM. Such transport patterns were already predicted and reported in the literature,[15] but are here clearly visualized for the first time.

Furthermore, it should be noted that a high-CO_2-concentration layer (ca. 5 μm thick) is formed at the interface between ZIF-8 and 6FDA-DAM polymer during the transient adsorption, colored in red in Figure 2. At equilibrium, more CO_2 molecules tend to reside in the interfacial region, compared to the bulk polymer phase. This phenomenon was even more pronounced at higher CO_2 pressures in the surrounding gas phase. Figure 3 shows separate images of CO_2 concentration in the ZIF-8@6FDA-DAM MMM at different equilibrium pressures at 308 K (see Supporting Information). The increased CO_2 concentration at the interface was seen to become more prominent as we shifted to higher equilibrium pressures.

To shed light on the causes of the CO_2 accumulation at the interface, two sets of molecular simulations have been performed. First, the MOF/polymer interface was modeled by applying a recently developed methodology[2a] that relies on density functional theory (DFT) and force-field based calculations. These simulations allowed us to obtain a microscopic description of the structural features that characterize the MOF/polymer interface. As a second step, the preferential location of adsorbed CO_2 in this MOF/polymer model was identified by means of grand canonical Monte Carlo (GCMC) simulations.
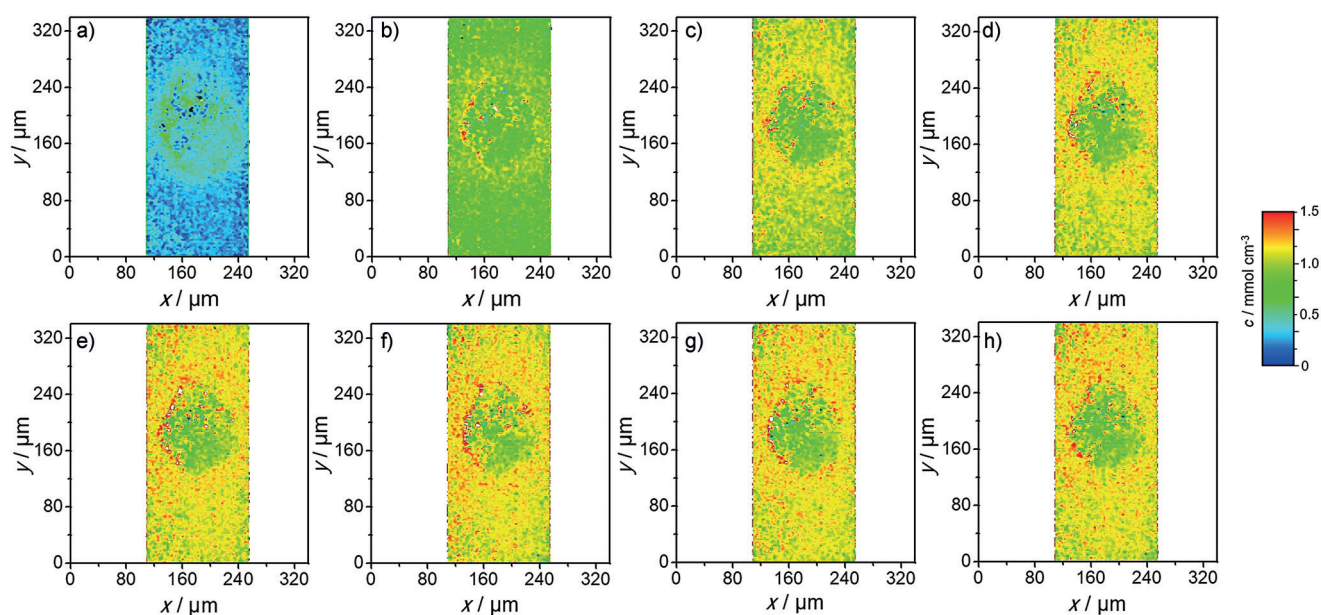

Figure 1. A big ZIF-8 crystal embedded in 150 μm-thick 6FDA-DAM polymer is placed in the measurement window (ca. 145 μm × 340 μm size) and subjected to microimaging via IR microscopy. a) The ZIF-8@6FDA-DAM MMM under the microscope in Viewing Mode. b) Color-filled contour map of ZIF-8 content in absence of CO_2. The increase of ZIF-8 content is indicated by the color change from blue to red.

Figure 2. Consecutive, time-resolved images of CO_2 concentration in the ZIF-8@6FDA-DAM MMM during CO_2 uptake driven by a pressure step from 0 to 400 mbar at 308 K. Each image is an averaged image of 8 scans captured during a) 3–27 s, b) 69–93 s, c) 130–154 s, d) 183–207, e) 237–261 s, f) 291–315 s, g) 344–368 s, and h) 415–439 s after the commencement of the CO_2 uptake. The increase in the CO_2 concentration is indicated by the color change from blue to red.
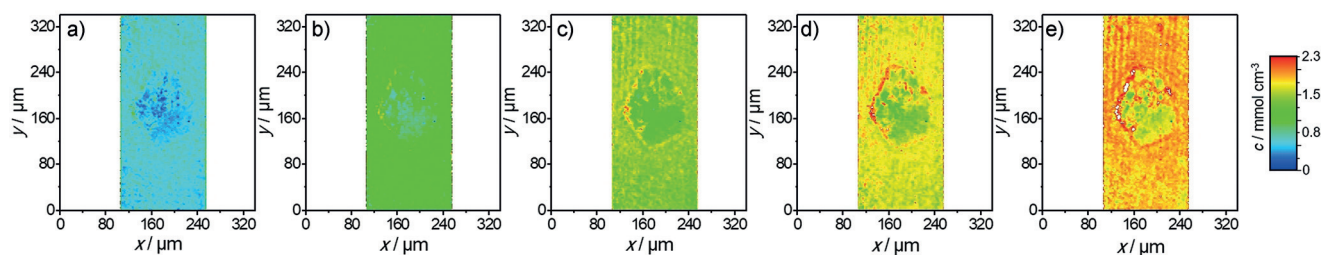

Figure 3. Separate images of CO_2 concentration in the ZIF-8@6FDA-DAM MMM at different pressures: a) 200 mbar, b) 400 mbar, c) 600 mbar, d) 800 mbar, e) 1000 mbar of CO_2 at 308 K. Each image is an averaged image of 64 scans captured at equilibrium. The increase of the CO_2 concentration is indicated by the color change from blue to red.

A previously DFT-optimized ZIF-8 [011] surface model[2a] was combined with a polydisperse 6FDA-DAM model generated by an in silico polymerization procedure.[16] The polymer was modeled as a flexible collection of charged Lennard-Jones (LJ) sites with bonds, angles and dihedral energy potential parameters taken from the general amber force field,[17] charges computed at the DFT-level and 12-6 LJ interatomic potential parameters taken from the TraPPE[18] potential as already used for other polymers.[2a,19] The model, consisting of several chains ranging between 9 and 37 mono-mers, was validated by a very good agreement between simulated density and X-ray scattering pattern and the corresponding experimental data (see Supporting Informa-tion and Figure S6). This model was subsequently combined with that for the ZIF-8 surface model through a series of molecular dynamics (MD) simulations that included changes in temperature and pressure to allow the polymer to adapt its configuration to the external field imposed by the chemistry and morphology of the MOF surface.[2a] Finally, structural data were collected from 10 statistically independent MD runs, spanning 10 ns each. The interface was found to be inhomogeneous at the nanometer scale, consisting of well-defined microvoids that are delimited by anchoring points resulting from weak interactions between the -NH and -OH terminations at the ZIF-8 surface and the -CH$_3$, -CF$_3$, and -CO groups of 6FDA-DAM (see Figure 4a, Figure S8 and Supporting Information). Figure 4b shows the atomic density of 6FDA-DAM as a function of the distance from the ZIF-8 surface along the z-direction (note that here the z-direction corresponds to the direction perpendicular to the MOF surface). In the closer proximity to the surface the atomic density of the polymer drops to zero (Region A). This step-change which occurs along the first nanometer of the surface $(9 \pm 1 \text{ Å})$ is a consequence of the presence of the microvoids at the interface, of up to 9 Å diameter (see details in Supporting Information and Figure S7). These microvoids are large enough to accommodate CO_2 molecules, and might be the origin of the CO_2 injection from the MOF into the polymer, as discussed above. The prediction of the presence of microvoids is further supported by solid-state nuclear
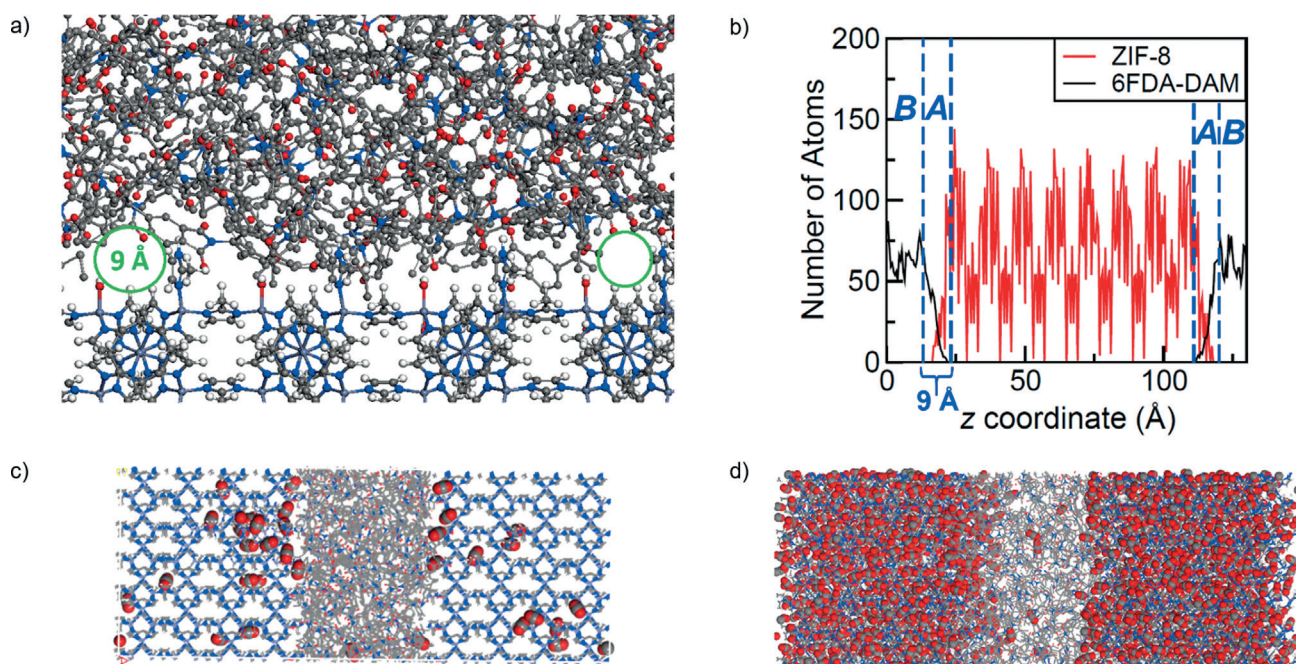
Figure 4. a) Representative snapshot of the interface in which microvoids can be seen (C gray, O red, N blue, H white). b) Atomic density of ZIF-8 and 6FDA-DAM as a function of the coordinate perpendicular to the ZIF-8 surface, c),d) Representative configurations of the loaded MMM models at low and high pressure, respectively.

magnetic resonance (SSNMR) experiments (see Supporting Information). The ^{13}C-^1H HETCOR (heteronuclear correlation) spectrum of the ZIF-8@6FDA-DAM MMM revealed the absence of strong interactions between the filler and the polymer, thereby implying poor compatibility of the two components (Figures S9–S11). Above a distance of 5 Å away from the last atom of the MOF surface, the atomic density of polymer fluctuates around more or less a constant value (Region B), which still differs from that of the bulk polymer. This means that the polymer in Region B still feels the impact of the MOF surface and a larger length along the *z*-direction would be required to mimic a bulk-like behavior at longer separating distances, as previously evidenced for the HKUST-1/PVOH[2b] composite. Regions A and B describe the MOF/polymer interface and its first-neighbor environment, respectively, and consequently they only constitute a tiny part of the high CO_2 concentration region found at the border of the MOF nanoparticle (nanometers versus micrometers).

To confirm that the CO_2 molecules can reside in the microvoids, GCMC simulations were further performed to explore the preferential sittings of CO_2 into the atomistic composite model. Two different CO_2 pressures were explored: 0.15 and 30 bar to model the first adsorption stage and the saturation regime, respectively. The CO_2 molecule was described by a charged LJ 3-sites model[20] while all atoms of the MOF model were treated with charged LJ sites with parameters taken from the UFF[21] force field. The CO_2 molecules were found to be primarily located both in the ZIF-8 pores and in the microvoids present at the MOF/polymer interface (Figures 4c,d). These results thus provide microscopic insight into the structural features that give rise to the first stages of the generation of the high CO_2

concentration region at the ZIF-8/6FDA-DAM interface. It is important to remark that the high CO_2 concentration region extends experimentally up to the micrometer scale, while the microvoids we describe are of sub-nanometric dimensions. We thus propose that the filling of the microvoids is only the first step in a mechanism that must also involve other transfer phenomena at the mesoscopic scale that cannot be currently investigated with our atomistic-based models.[2b]

In summary, microimaging by IR microscopy has been applied to record the evolution of CO_2 concentration in the ZIF-8@6FDA-DAM mixed-matrix membrane (MMM). To our knowledge, such a type of measurements visualizing the difference in "localized" CO_2 concentration between the polymer and the filler has never been achieved so far. We have demonstrated from the time-resolved images that the CO_2 molecules propagate from the filler, which appears to act as a "highway" for CO_2 mass transport, to the surrounding polymer. We have also observed the enhancement of CO_2 concentration at the interface between the polymer and the filler at equilibrium. This phenomenon becomes even more pronounced at higher gas pressures. A microscopic explanation of the first stages of this phenomenon has been provided by means of atomic simulations, which have evidenced the presence of microvoids at the MOF/polymer interface. GCMC simulations have shown that the accumulation of CO_2 molecules is favored in these microvoids, which could constitute the first step in the mechanism of the formation of the high CO_2 concentration layer at the interface with the MOF and further support the importance of filler-polymer compatibility in MMM performance.

In future studies, the CO_2 transport diffusivity in the same MMM should be measured by following the "diffusion front"

that may propagate from an open edge of a surface-coated MMM towards its interior in which fillers are located. After calculating the diffusivity, the Maxwell model,[8] which is often considered as the most appropriate model to predict MMM behavior especially for MMMs with low volume fractions of filler,[4,22] may be applied to study its validity in the present MMM.

Acknowledgements

Conflict of interest

The authors declare no conflict of interest.

[1] a) B. Seoane, J. Coronas, I. Gascon, M. E. Benavides, O. Karvan, J. Caro, F. Kapteijn, J. Gascon, *Chem. Soc. Rev.* **2015**, *44*, 2421–2454; b) B. Seoane, S. Castellanos, A. Dikhtiarenko, F. Kapteijn, J. Gascon, *Coord. Chem. Rev.* **2016**, *307*, 147–187.

[2] a) R. Semino, N. A. Ramsahye, A. Ghoufi, G. Maurin, *ACS Appl. Mater. Interfaces* **2016**, *8*, 809–819; b) R. Semino, J. P. Dürholt, R. Schmid, G. Maurin, *J. Phys. Chem. C* **2017**, *121*, 21491–21496; c) R. Semino, J. C. Moreton, N. A. Ramsahye, S. M. Cohen, G. Maurin, *Chem. Sci.* **2018**, *9*, 315–324.

[3] a) J. Kärger, T. Binder, C. Chmelik, F. Hibbe, H. Krautscheid, R. Krishna, J. Weitkamp, *Nat. Mater.* **2014**, *13*, 333–343; b) T. Titze, C. Chmelik, J. Kullmann, L. Prager, E. Miersemann, R. Gläser, D. Enke, J. Weitkamp, J. Kärger, *Angew. Chem. Int. Ed.* **2015**, *54*, 5060–5064; *Angew. Chem.* **2015**, *127*, 5148–5153; c) T. Titze, A. Lauerer, L. Heinke, C. Chmelik, N. E. R. Zimmermann, F. J. Keil, D. M. Ruthven, J. Kärger, *Angew. Chem. Int. Ed.* **2015**, *54*, 14580–14583; *Angew. Chem.* **2015**, *127*, 14788–14792.

[4] R. Mahajan, W. J. Koros, *Polym. Eng. Sci.* **2002**, *42*, 1420–1431.

[5] R. Mahajan, W. J. Koros, *Polym. Eng. Sci.* **2002**, *42*, 1432–1441.

[6] a) J. Berriot, H. Montes, F. Lequeux, D. Long, P. Sotta, *EPL* **2003**, *64*, 50; b) J. H. Petropoulos, K. G. Papadokostaki, F. Doghieri, M. Minelli, *Chem. Eng. Sci.* **2015**, *131*, 360–366.

[7] a) L. E. Nielsen, *Ind. Eng. Chem. Fundam.* **1974**, *13*, 17–20; b) L. Rayleigh, *Philos. Mag.* **1892**, *34*, 481–502; c) M. Minelli, F. Doghieri, K. G. Papadokostaki, J. H. Petropoulos, *Chem. Eng. Sci.* **2013**, *104*, 630–637.

[8] J. C. Maxwell, *A treatise on electricity and magnetism*, Clarendon, Oxford, **1873**.

[9] C. Chmelik, H. Bux, J. Caro, L. Heinke, F. Hibbe, T. Titze, J. Kärger, *Phys. Rev. Lett.* **2010**, *104*, 085902.

[10] a) J. van den Bergh, J. Gascon, F. Kapteijn, in *Zeolites and Catalysis* (Eds.: J. Čejka, A. Corma, S. Zones), Wiley-VCH, Weinheim, **2010**, pp. 361–387; b) J. Kärger, D. M. Ruthven, D. N. Theodorou in *Diffusion in Nanoporous Materials*, Wiley-VCH, Weinheim, **2012**, pp. 25–58; c) J. Kärger, D. M. Ruthven, *New J. Chem.* **2016**, *40*, 4027–4048.

[11] C. Zhang, Y. Dai, J. R. Johnson, O. Karvan, W. J. Koros, *J. Membr. Sci.* **2012**, *389*, 34–42.

[12] A. Sabetghadam, B. Seoane, D. Keskin, N. Duim, T. Rodenas, S. Shahid, S. Sorribas, C. Le Guillouzer, G. Clet, C. Tellez, M. Daturi, J. Coronas, F. Kapteijn, J. Gascon, *Adv. Funct. Mater.* **2016**, *26*, 3154–3163.

[13] P. R. Griffiths, J. A. de Haseth, *Fourier Transform Infrared Spectroscopy*, Wiley, New York, **1986**.

[14] A. Pusch, T. Splith, L. Moschkowitz, S. Karmaker, R. Biniwale, M. Sant, G. B. Suffritti, P. Demontis, J. Cravillon, E. Pantatosaki, F. Stallmach, *Adsorption* **2012**, *18*, 359–366.

[15] D. Schneider, D. Mehlhorn, P. Zeigermann, J. Kärger, R. Valiullin, *Chem. Soc. Rev.* **2016**, *45*, 3439–3467.

[16] L. J. Abbott, K. E. Hart, C. M. Colina, *Theor. Chem. Acc.* **2013**, *132*, 1334.

[17] J. Wang, R. M. Wolf, J. W. Caldwell, P. A. Kollman, D. A. Case, *J. Comput. Chem.* **2004**, *25*, 1157–1174.

[18] B. L. Eggimann, A. J. Sunnarborg, H. D. Stern, A. P. Bliss, J. I. Siepmann, *Mol. Simul.* **2014**, *40*, 101–105.

[19] G. S. Larsen, P. Lin, K. E. Hart, C. M. Colina, *Macromolecules* **2011**, *44*, 6944–6951.

[20] J. G. Harris, K. H. Yung, *J. Phys. Chem.* **1995**, *99*, 12021–12024.

[21] A. K. Rappe, C. J. Casewit, K. S. Colwell, W. A. Goddard, W. M. Skiff, *J. Am. Chem. Soc.* **1992**, *114*, 10024–10035.

[22] R. M. Barrer, J. H. Petropoulos, *Br. J. Appl. Phys.* **1961**, *12*, 691.